[AMERICAN JOURNAL OF SCIENCE, VOL. 296, DECEMBER, 1996, P. 1093–1125]

American Journal of Science

DECEMBER 1996

CIRCULATION, SALINITY, AND DISSOLVED OXYGEN IN THE CRETACEOUS NORTH AMERICAN SEAWAY

PAUL W. JEWELL
Department of Geology and Geophysics,
University of Utah,
Salt Lake City, Utah 84112

ABSTRACT. Critical paleoceanographic problems regarding the maximum transgressive phase of the Cretaceous North American seaway have been studied with a three-dimensional ocean circulation model. Four simulations employing minimum and maximum solar insolation winds from the Cretaceous and a wide range of precipitation—evaporation (P–E) rates have been conducted. Winter, minimum solar insolation winds are similar to modern zonal wind patterns and produce a subtropical gyre with a strong western boundary current and broad, easterly return flow. Winter and summer maximum solar insolation winds and summer minimum solar insolation winds do not have significant wind stress curl and produce western and eastern boundary currents of equal intensity. Residence time of shallow (<100 m) water ranges from 0.6 to 2.5 yrs while deep water mass residence time varies from 1.3 to 4.6 yrs. Maximum vertical salinity differences within the seaway are approx 3 permil (10 percent freshwater dilution) when average P–E is ~1.5 m/yr and 6 permil (20 percent freshwater dilution) when P–E is ~3.5 m/yr. Relatively short surface water residence times prevent significant freshening of surface water. The influence of freshwater from rivers discharging at the western boundary is not pronounced due to limited drainage area and the strong western boundary currents. Dissolved oxygen has been modeled by assuming a productivity of 100 gC m^{-2}/yr throughout the seaway and employing empirical carbon flux-depth relationships from the modern ocean in conjunction with Redfield O_2:C ratios. Apparent oxygen utilization is modest (<20 μmol/kg) for all simulations due to the short deep water residence times in the seaway. The numerical simulations and simple box model calculations suggest that the widely documented anoxic episodes of the transgressive Cenomanian-Turonian North American seaway are a result of incursions of mid-depth, suboxic, or anoxic water from the open ocean or restricted deep water circulation due to a sill at the seaway entrance. Brackish surface water caused by elevated precipitation prevents mixing of oxygenated water from the surface although other factors (deep water residence time, water depth, and magnitude of biological productivity) determine whether anoxia develops in the deep seaway waters.

INTRODUCTION

The Middle to Late Cretaceous period of earth history is characterized by high sea level stands brought about by a global increase in sea floor spreading rates (Hancock and Kauffman, 1979; Kominz, 1984). As a result, the interiors of some continents were flooded by epiric seas. Among the most prominent and well-studied of these is the Cretaceous North American Seaway which existed from early Late Albian to Maestrichtian time. During periods of maximum transgression, the seaway extended nearly 5000 km in a north-south direction, was more than 1000 km wide, and connected the Arctic Ocean with the Gulf of Mexico (Williams and Stelck, 1975).

Observational and numerical modeling studies have shed considerable light on climatological conditions that may have been present in the Cretaceous North American Seaway. Paleobiological reconstructions (Kaufmann, 1984) and numerical model studies (Barron and Washington, 1982) suggest that climate over the seaway was strongly influenced by the circum-equatorial Tethyan Sea to the south. Precipitation over North America is believed to have been enhanced by the thermal contrast between the Tethyan Ocean and the North American continent (Barron and Washington, 1982; Barron, Arthur, and Kauffman, 1985). Atmospheric general circulation (GCM) model studies suggest that precipitation over western North America was particularly intense (up to 5.0 m/yr) with somewhat smaller average precipitation (approx 1.5 m/yr) over eastern North America (Barron and Washington, 1982).

Pelagic rocks deposited in the deepest portion of the Cretaceous North American Seaway during transgressive periods show well-defined limestone-shale couplets which are believed to be related to cyclic changes in planetary orbital parameters (Barron, Arthur, and Kauffman, 1985). The bioturbated limestones appear to have been deposited in an oxygenated bottom water environment, whereas the organic carbon-rich shales were probably the result of anoxic bottom waters in the seaway (Pratt, 1984). Complicating overall understanding of the redox conditions during transgressive phases of the seaway are oceanwide anoxic events during the Cenomanian-Turonian (Schlanger and Jenkyns, 1976). Water from the oxygen-minimum zone of the open ocean would have been likely to enter the seaway, thereby causing or at least enhancing seaway anoxia. Atmospheric GCM studies suggest that variations in orbital parameters exerted a major influence on seasonal precipitation intensity and hence bottom water anoxia (Glancy and others, 1993). During periods of maximum solar insolation, enhanced ocean-continent thermal contrast leads to greater precipitation (up to 2.2 m/yr increase) over the seaway relative to minimum solar insolation conditions.

A large number of features concerning the Cretaceous North American Seaway remain controversial despite over a century of research. Foremost among these is the role that freshwater played in causing anoxic bottom water during maximum transgressions in the seaway. One school of thought attributes the anoxia to high precipitation and associ-

ated river runoff which created a brackish-water lid on the seaway surface (Pratt, 1984; Arthur and others, 1985). Evidence for this theory comes largely from the depleted oxygen isotope signatures of carbonates deposited during the maximum transgression. The brackish-water lid model appears to be contradicted by paleontological data which suggests that the seaway had near normal salinity during this period of time (Eicher and Diner, 1985).

Mesoscale ocean circulation models are a potentially effective tool for studying the hydrographic conditions of ancient marine environments such as the Cretaceous Interior Seaway. Mesoscale models (generally defined as having grid spacing of less than 100 km) have been used to examine biogeochemical (Hoffman, 1988; Walsh, Dieterle, and Meyers, 1988) and sedimentary (Sheng and Lick, 1979; Graber, Beardsley, and Grant, 1989; Jewell, Stallard, and Mellor, 1993) processes in modern coastal oceans. Mesoscale models of the Cretaceous North American Seaway have been used to study tides (Slater, 1982) and the relationship between velocity fields and sedimentology (Eriksen and Slingerland, 1990).

In this study, a mesoscale hydrodynamic model is used to test various scenarios of the hydrography and paleoclimatology of the Cenomanian-Turonian transgressive phase. This work is intended to address several key questions: (1) What are the consequences of different wind circulation patterns on seaway hydrography? (2) What precipitation, evaporation, and river runoff scenarios are necessary to produce surface water salinities suggested by the oxygen isotope analyses of rocks deposited during the Cenomanian-Turonian transgression? (3) What is the rate of oxygen utilization within the seaway, and what is its relation to contemporaneous global anoxic events?

Many of these questions were addressed in a preliminary, one-dimensional model of seaway dynamics (Jewell, 1993). The present study was undertaken to test the conclusions of that study in a more vigorous and systematic manner. The seaway bathymetry and relevant physical parameters are represented within an idealized framework, rather than attempting to reproduce specific details of Cenomanian-Turonian paleogeography and paleoceanography. The study was undertaken in the spirit of determining the role that specific physical controls (wind stress patterns and precipitation-evaporation) have on salinity and oxygen concentrations in this unique geological environment.

MODEL DESCRIPTION

Model domain and bathymetry.—Numerical experiments employed a domain representing the simplified paleogeography of western North America during the Cenomanian-Turonian transgression (approx 90–95 my BP). During this period of time, the seaway was connected with both the Arctic Ocean and the Gulf of Mexico and may also have extended into what is now Hudson Bay (Kaufmann, 1984). The model domain of this study includes the southern 2200 km of the approx 5000 km total length

of the Cenomanian-Turonian seaway (fig. 1). The model extends from 33° to 53°N paleolatitude. Most paleogeographic reconstructions of the Cenomanian-Turonian seaway show a broad opening at the Gulf of Mexico (Kaufmann, 1984; Funnel, 1990). A linear opening to the Gulf of Mexico was used in this study in order to facilitate numerically tidal forcing at the southern boundary (fig. 1A). This simplification would not be expected to alter significantly the physical and geochemical simulations of the interior of the model domain north of 37°N. Some researchers have suggested that the southern entrance to the seaway was restricted by a carbonate bank during the Albian (Kaufmann, 1984; Winker and Buffler, 1989). During the Cenomanian-Turonian transgression, both paleontologists and modelers suggest that the seaway had well-established connections with the Tethyan ocean (Kaufmann, 1984; Eriksen and Slingerland, 1990).

Bathymetry of the model domain is a simplified variation of the asymmetric foreland basin described by Kaufmann (1984). Maximum depth of the foreland trough is assumed to be 400 m. The asymmetry of the basin is believed to be the result of tectonic thrusting and mountain building in the Sevier orogenic highlands to the west. These mountains are also believed to have caused enhanced river runoff and sediment delivery from the west (Eaton and Nations, 1991). Low-lying lands to the east in what is now the central United States are characterized by relatively low sedimentation rates (Kaufmann, 1984).

The idealized, asymmetric basin shape is maintained throughout the entire model domain (fig. 1B). The idealized shape is not considered critical since the primary purpose of this study is an understanding of factors that control salinity and oxygen in the water column, rather than modeling specific paleogeographic features and depositional environments of the seaway.

The numerical model.—The mesoscale circulation model used in this study is the so-called Princeton Ocean Model (POM). POM is rapidly becoming one of the standard hydrodynamic tools of the coastal ocean modeling community (American Society of Civil Engineers, 1988; Conner, 1991) on the basis of its proven track record of accurately simulating velocity, temperature, and salinity fields in estuaries (Oey, Mellor, and Hires, 1985; Galperin and Mellor, 1990; Jewell, Stallard, and Mellor, 1993), the open ocean (Mellor and Ezer, 1991; Ezer and Mellor, 1992), and sea-ice domains (Mellor and Kantha, 1989; Hakkinen and Mellor, 1990). One-dimensional versions of POM have been used to model dissolved oxygen in lakes (Jewell, 1992) and the Cretaceous North American Seaway (Jewell, 1993).

One of the key features of POM is its realistic formulation of vertical eddy viscosity and diffusivity through the use of the "Level 2.5" turbulence closure model of Mellor and Yamada (1974, 1982). Accurate, real-time simulation of these variables is critical for studying stratified conditions such as those present in epicontinental seaways. Details of the numerical implementation of POM can be found in Blumberg and Mellor

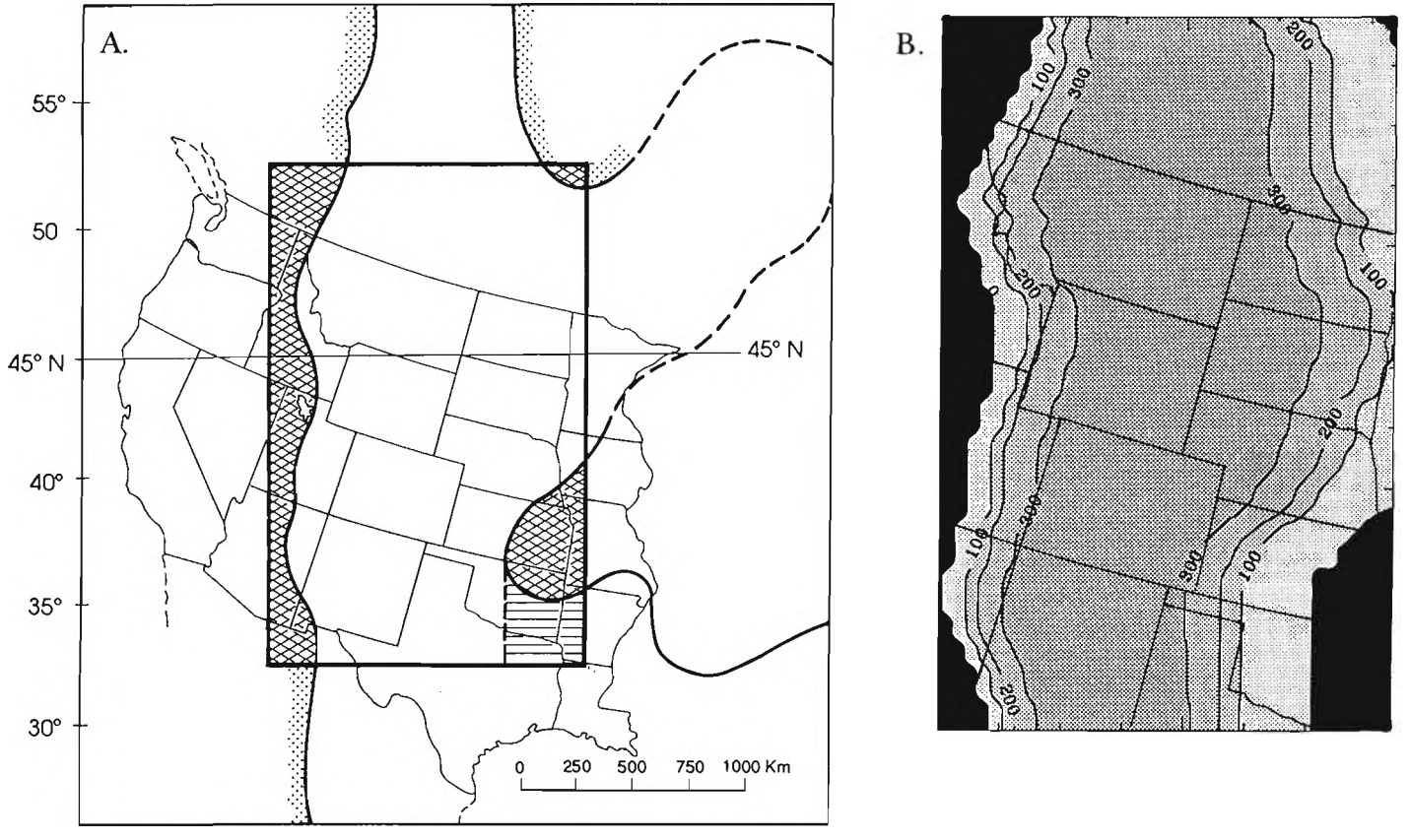

Fig. 1(A) Paleogeography and areal model domain for simulations of Cretaceous Interior during the Cenomanian-Turonian transgression (from Kaufmann, 1984). Dark areas represent land points in the model domain. Cross-hatched zone is an area considered to be open ocean in most paleogeographic reconstructions but modeled as land in this study in order to facilitate numerical simulation of tides. (B) Idealized bathymetry of the model domain showing an asymmetric foreland trough basin.

(1987). Conservation equations are solved for momentum, heat, salt, turbulent kinetic energy, and turbulence macroscale. The latter two variables are used to determine vertical eddy viscosity and diffusivity through a series of analytic stability functions that contain a small number of empirical laboratory turbulence constants. Horizontal eddy viscosity and diffusivity are computed with the formulation of Smagorinsky (1963). Numerical implementation is accomplished with a finite difference scheme which is explicit in the horizontal and implicit in the vertical directions. Time-step differencing is by a leap-frog technique (Roach, 1982).

The model employs a σ-coordinate system in which grid points are scaled to the depth of the water column at any given point.

$$\sigma = \frac{z - \eta}{H + \eta} \tag{1}$$

H is total water depth, and η is the free surface elevation. $\sigma = 0$ at the free surface, and $\sigma = -1$ at the bottom ($z = H$). The simulations employed in this study used 11 σ levels which are logarithmic at the surface and equally spaced throughout the rest of the water column (table 1). The horizontal finite difference grid is staggered with the velocity and turbulence variables being offset by one-half grid point from variables for surface elevation, temperature, and salinity. This arrangement has been shown to be very effective for ocean models with horizontal grid spacings lower than 50 km (Bateen and Han, 1981).

TABLE 1

Summary of σ layers used in the model

Level	σ
1	0.000
2	−0.031
3	−0.063
4	−0.125
5	−0.250
6	−0.375
7	−0.500
8	−0.625
9	−0.750
10	−0.875
11	−1.000

POM employs a split time step whereby the depth-averaged, two-dimensional (external) portion of the model is solved with relatively short time steps, and the full, three-dimensional (internal) portion of the model is solved using a much longer time step. The external time step is set according the Courant-Friedrich-Levy (CFL) stability constraint.

$$\Delta t \leq \frac{1}{C_t}\left(\frac{1}{\Delta x^2} + \frac{1}{\Delta y^2}\right)^{-1/2} \tag{2}$$

C_t is the shallow water wave speed, $(gH)^{1/2}$. The internal time step is set to a multiple of the external time step which is dependent on the internal wave speed, $C_i \sim (gH\Delta\rho/\rho)^{1/2}$ where $\Delta\rho$ is the maximum vertical density gradient.

In this model, the horizontal grid spacing was set to 33.3 km in both the x- and y-directions. This grid spacing was the maximum that could be used in conjunction with the horizontal viscosity formulation of Smagorinsky (1963) without inducing subgrid oscillations (Roach, 1982, p. 41). The external time step was 166 s. The internal time step was 18 times the external time step (that is 49.8 min) for all but the highest precipitation (and hence vertical density gradient) simulations. In this case, the internal time step was 9 times the external time step.

A simple series of calculations were used to simulate dissolved oxygen in the seaway. Oxygen concentrations were set to saturation values at the beginning of each simulation according to the polynomial dissolved oxygen–temperature–salinity relationship of Carpenter (1966). Oxygen concentrations below 100 m were determined from empirical carbon flux-depth relationships. Although a variety of these expressions has been established from sediment trap observations in the ocean (Berger, Smetacek, and Wefer, 1989; Bishop, 1989), the best fit of observations at <1000 m depth was chosen for this study (Berger, Smetacek, and Wefer, 1989).

$$J(z) = \frac{6.3PP}{z^{0.8}} \tag{3}$$

J is organic carbon flux (gC m^{-2} yr^{-1}), PP is primary productivity (also in gC m^{-2} yr^{-1}), and z is depth. For a given depth interval, the change in carbon flux was converted to an equivalent amount of oxygen consumption using Redfield ratios from the modern ocean (Takahashi, Broecker, and Langer, 1985). Any carbon flux to the sediments was remineralized and subtracted as an equivalent amount of oxygen in the bottom-most grid point. This is in accordance with observations from the modern ocean that only a small fraction of organic carbon reaching the seafloor becomes permanently sequestered in the sediments (Emerson and Hedges, 1988).

A uniform primary production value of 100 gC m^{-2} yr^{-1} was used for all the simulations presented here. This is within the range calculated by Pratt (1985) for a variety of Cenomanian-Turonian sections in the seaway. Pratt's estimate of productivity in turn is based on empirical productivity-carbon accumulation relationships of modern sediments presented by Bralower and Thierstein (1984). Upwelling within various portions of the seaway has been invoked as a mechanism for anoxic water and organic-rich sediments (Glancy and others, 1993; Hay, Eicher, and Diner, 1993) as well as the formation of the phosphate-rich Sharon Springs Member of the Pierre Shale of Campanian age (Parrish and Gautier, 1993). Upwelling typically produces primary productivity rates much higher than those used in this model. In the "Discussion" section

below, possible implications of higher primary productivity are considered.

Model physics at the boundaries.—Circulation in the Cretaceous Interior Seaway was no doubt strongly influenced by tides. Tidal forcing in this study was accomplished by changing the elevation over the period of a modern M_2 (12.42 hrs) tidal cycle by an amplitude of 0.25 m at the southern (Gulf of Mexico) boundary. The surface elevation boundary condition at the northern (Arctic Ocean) boundary was calculated with a centered, explicit radiation boundary condition which allows surface waves to propagate through the domain without reflection (Kantha, Blumberg, and Mellor, 1990). Two previous numerical modeling studies have addressed the role that tides played in the sedimentation and hydrography of the seaway (Slater, 1985; Eriksen and Slingerland, 1990). Results of this study were similar to these previous studies, and so the role of tides is not discussed in this paper.

The surface momentum flux boundary condition is:

$$\rho_o K_M \left(\frac{\partial U}{\partial z}, \frac{\partial V}{\partial z} \right) = (\tau_{ox}, \tau_{oy}) \tag{4}$$

(τ_{ox}, τ_{oy}) is the surface wind shear stress, ρ_o is water density, and K_M is vertical eddy viscosity. Wind shear stress is calculated with the relationship:

$$\tau_a = \rho_a C_D V_a |V_a| \tag{5}$$

ρ_a is the density of air, and $|V_a|$ is the mean surface wind velocity. The drag coefficient, C_D, is calculated according to the relationships described by Large and Pond (1981).

$$C_D = .0012 \qquad 4 \leq V_a < 11 \text{ m/s} \tag{6A}$$

$$C_D = .00049 + .000065 V_a \qquad 11 \leq V_a < 25 \text{ m/s} \tag{6B}$$

Bottom boundary shear stress was determined by matching velocities with the logarithmic law of the wall.

$$\tau_b = \rho_w C_{Db} V_b |V_b| \tag{7}$$

V_b is the velocity at the bottom grid point of the model, and ρ_b is the bottom water density. The value of the bottom drag coefficient is computed as:

$$C_{Db} = \left[\frac{1}{\kappa} \ln (H + z_b)/z_o \right]^{-2} \tag{8}$$

κ is the von Karmen constant and assumed to be 0.4 (Blumberg and Mellor, 1987). H is water depth, and z_b is the depth of the grid point nearest to the bottom. z_o is the roughness length and depends on the local character of the bathymetry. In this study, z_o was set to 1 cm in a manner

similar to other applications (Weatherly and Martin, 1978; Blumberg and Mellor, 1987). In deep water where the bottom boundary layer is not well resolved vertically by the model, C_D is set to 0.0025. The POM code is written so C_D is the larger of this value or that calculated by (8).

Surface heat and salinity boundary conditions are set according to:

$$\rho_o K_H \left(\frac{\partial \Theta}{\partial z}, \frac{\partial S}{\partial z} \right) = \dot{H}, \dot{S} \tag{9}$$

K_H is vertical eddy diffusivity, Θ is temperature, S is salinity, $\dot{H}$ is surface heat flux, and $\dot{S}$ is surface salinity flux. Mean surface heat flux was specified according to averages in the Pacific Ocean (table 2) (Budyko, 1986). A seasonal heat flux amplitude of 50 W m^{-2} was superimposed on these averages. This produced seasonal sea surface temperature variations which approximated those of the modern Pacific Ocean (Piexoto and Oort, 1992).

TABLE 2

Summary of initial temperature and salinity conditions and surface heat flux boundary conditions used for all model runs

Parameter	Value
Northern surface temperature (°C)*	10
Southern surface temperature (°C)*	18
Nothern bottom temperature (°C)*	6
Southern bottom temperature (°C)*	9
Northern surface salinity (ppt)*	34
Southern surface salinity (ppt)*	36
Nothern bottom salinity (ppt)*	36
Southern bottom salinity (ppt)*	36
Mean northern surface heat flux (W m^{-2})**	−50
Mean southern surface heat flux (W m^{-2})**	25
Seasonal surface heat flux amplitude (W m^{-2})**	50

* Levitus (1982).
** Budyko (1986).

Inflowing tangential velocity, temperature, salinity, and oxygen at the open northern and southern boundaries were specified using the initial conditions described below. Outflowing boundary conditions are described according to the advection condition:

$$\frac{\partial C_i}{\partial t} + U_n \frac{\partial C_i}{\partial n} = 0 \tag{10}$$

n refers to the coordinate normal to the boundary, and C is the scalar quantity being considered.

MODEL DESIGN AND RUNS

Designing numerical simulations of a mesoscale oceanic domain requires specifying boundary values for wind, temperature, salinity,

surface heat flux, precipitation, and evaporation. In the case of the Cretaceous Interior seaway, these boundary values could be derived from modern analogs or from Cretaceous atmospheric or oceanic general circulation models (GCMs). A combination of these two possibilities is used in this study. Atmospheric GCM output is used for wind boundary conditions because different continental configurations would be expected to produce wind fields that differ from those of the modern atmosphere. In contrast to atmospheric GCM studies, only a small number of oceanic GCM simulations of the Cretaceous have been published (Barron and Washington, 1990). Furthermore, GCM simulations of the modern ocean have not been as successful as GCM simulations of the modern atmosphere (Haidvogal and Bryan, 1993). For these reasons, lateral temperature and salinity boundary values as well as surface heat flux were set to modern values close to those of the Pacific Ocean (table 2). Precipitation rates over the seaway are treated as an independent variable in order to test their effect on surface salinity.

Seaway wind patterns.—Surface wind boundary values for all the model runs were taken from an atmospheric GCM study of maximum and minimum solar insolation periods of the Cretaceous (Glancy, ms; Glancy and others, 1993). Minimum solar insolation is defined as the point at which Earth's orbital parameters (eccentricity of the elliptical orbit around the Sun and the obliquity and precession of Earth's rotational axis) cause Earth's northern hemisphere to receive a minimum amount of solar radiation during the northern hemisphere summer. During maximum solar insolation, the northern hemisphere receives the maximum possible solar radiation during the northern hemisphere summer.

The relatively small number of grid points overlying the seaway in the atmospheric GCM model were interpolated with a bicubic spline routine to obtain smoothly varying wind stress fields. Winter minimum insolation winds have a pattern similar to that of the modern northern hemisphere, that is, westerly flow north of paleolatitude 35°N and weak easterly flow south of this point (fig. 2, 3A), although the north-south wind gradients are weaker than those observed in the modern atmosphere (fig. 2). Summer-minimum insolation winds have a strong northerly component in the northern part of the domain and a weak southerly component in the south (fig. 3B). Wind magnitude for both seasons during minimum solar insolation does not exceed 7 m/s, with the strongest winds occurring in northern latitudes during the summer.

Maximum insolation winter winds are largely southerly (fig. 3C) and do not show the zonal gradients of the minimum insolation winds (fig. 2). Maximum insolation summer wind patterns (fig. 3D) resemble those of the minimum insolation summer winds (fig. 3B). Both summer and winter maximum insolation winds are more intense than contemporaneous minimum insolation winds. This is attributed to increased ocean-land thermal contrast in the maximum insolation GCM simulations (Glancy and others, 1993).

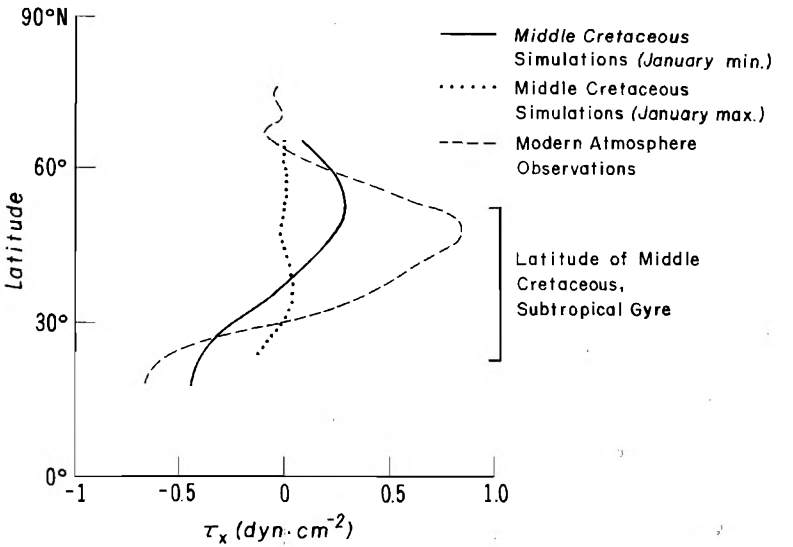

Fig. 2. East-west wind-shear stress patterns (in dynes/cm^2) for the Cretaceous atmosphere (Glancy, 1992) and the modern atmosphere (Hellerman and Rosenstein, 1983). January minimum and January maximum refer to the amount of solar insolation applied during Cretaceous winter general circulation model simulations. Cretaceous wind stress is average of values over the seaway: modern zonal average of world atmosphere.

Initial temperature and salinity.—Initial temperature and salinity fields were set close to those of the modern Pacific Ocean (table 2) (Levitus, 1982). Although Cretaceous sea suface temperatures may have been somewhat higher (Barron and Peterson, 1990), this would not have had a major influence on questions regarding salinity and oxygen investigated in this study. Surface salinity was set to 34 ppt at the northern boundary and 36 ppt at the southern boundary (table 2). The northern salinity value is higher than that hypothesized by Hay, Eicher, and Diner (1993) who argue that the salinity of the Cretaceous Arctic Ocean was similar to that of the modern Arctic Ocean (that is ~30 ppt) (Pickard and Emery, 1982). The relatively low salinity of the modern Arctic Ocean is the result of discharge from several large rivers and restricted exchanges with the modern Atlantic and Pacific Oceans. Paleogeographic reconstructions of the Cretaceous show that the connection between the Arctic and Pacific Ocean was quite wide (Funnel, 1990). During high sealevel stands, the depth of this connection was almost certainly greater than the depth of the modern Bering Straits, and water exchange between the two oceans was almost certainly greater than it is today.

A variety of researchers believe that a strong zonal temperature or salinity front existed within the seaway. Much of the evidence for a front is paleobiologic (Hay, Eicher, and Diner, 1993; Fisher, Hay, and Eicher, 1994). Such a front would most likely be the result of strongly contrasting

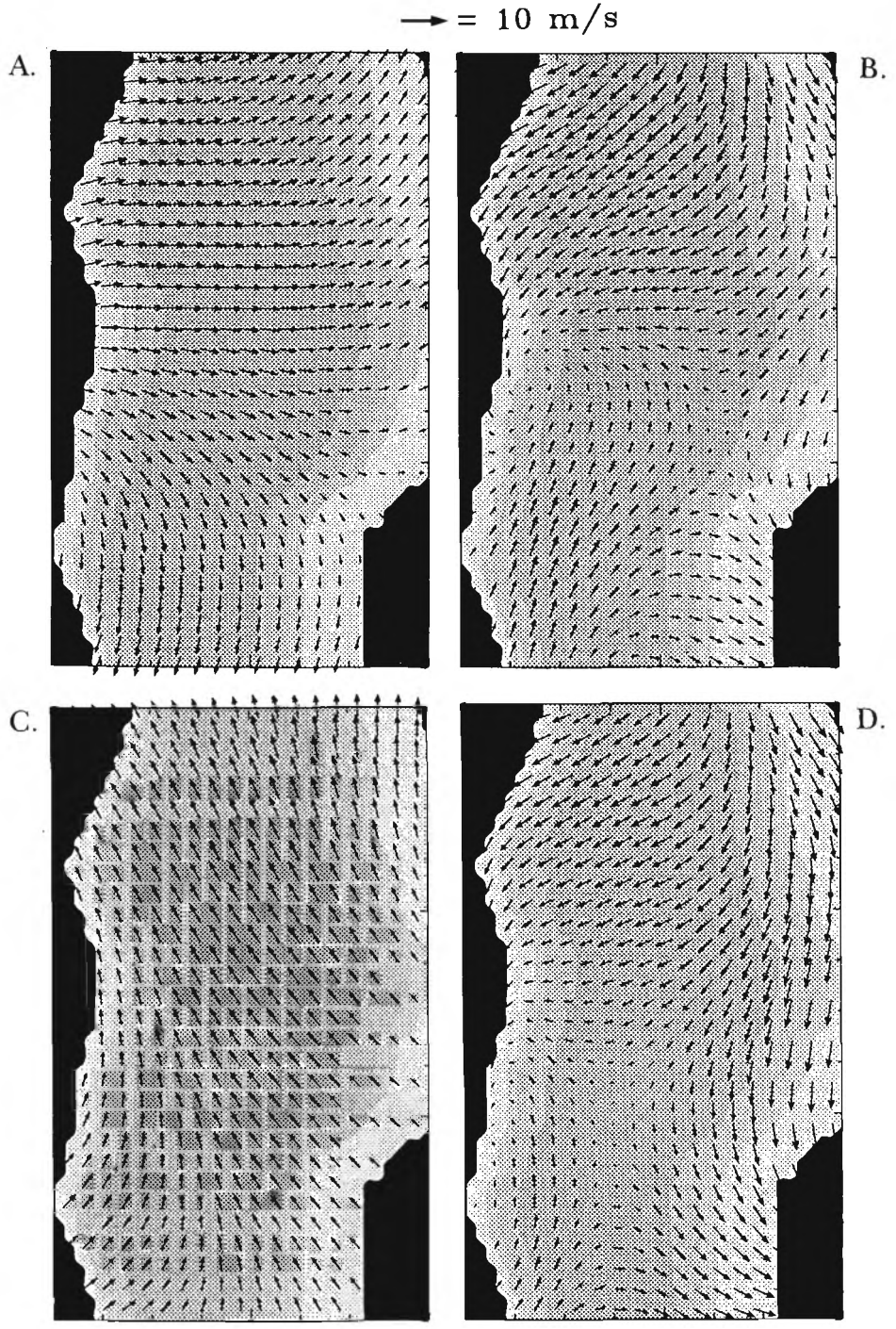

Fig. 3. Wind vectors used as boundary conditions for Cretaceous simulations (interpolated from the GCM results of Glancy (1992)). (A) Minimum solar insolation winter winds; (B) minimum solar insolation summer winds; (C) maximum solar insolation winter winds; (D) maximum solar insolation summer winds.

thermal or salinity characteristics of the northern and southern water masses. The simulations in this study were not aimed at reproducing a front within the seaway. Instead the emphasis here is on understanding the wind driven circulation, surface and deep water residence times, and the oxygen utilization in the deep waters of the seaway as a function of simplified initial temperature and salinity conditions.

Precipitation, evaporation, and river runoff.—Precipitation minus evaporation (P–E) to the surface of the seaway was applied according to eq (9) and varied according to the specific model runs described below (table 3). Atmospheric GCM studies have suggested that precipitation may have varied seasonally due to the monsoon effect of the Sevier highlands (Glancy and others, 1993). For this study, precipitation was not varied, and the overall effect of seasonally varying precipitation rates was not examined.

TABLE 3

Summary of precipitation and evaporation boundary conditions for the model runs (in units of m/yr). Modern precipitation, evaporation values are from Piexoto and Oort (1992).

	Northern Precipitation	Southern Precipitation	Northern Evaporation	Southern Evaporation
Simulation A: Cretaceous winds (minimum insolation) Modern P–E	0.7	0.8	0.6	1.2
Simulation B: Cretaceous winds (maximum insolation) Modern P–E	0.7	0.8	0.6	1.2
Simulation C: Cretaceous winds (maximum insolation) Moderate P–E	2.0	2.0	0.6	1.2
Simulation E: Cretaceous winds (maximum insolation) High P–E	4.0	4.0	0.6	1.2

River input to the western portion of the domain was modeled by increasing the precipitation at westernmost seaway gridpoint to 5 times the precipitation value elsewhere in the model domain (table 3). River inflow was therefore modeled as a series of regularly-spaced small rivers rather than a smaller number of large rivers. The justification and effect of this simplification are discussed in more detail below. The factor of 5 was determined by assuming that the distance to the crest of the Sevier highlands to the west was ten grid points (333 km) away and that the ratio of river runoff to precipitation was 0.5 (Holland, 1978). Note that this formulation does not take the orographic effect of the Sevier highlands into consideration. This may have increased precipitation rates over land. Nevertheless, comparison of this model with modern river basins (discussed below) suggests that formulating river runoff in this manner is valid.

Model runs.—Four model runs were conducted (table 3). The numerical experiments were meant to encompass wide variations in wind and P–E conditions during the Cenomanian-Turonian period. Simulation A employed P–E boundary conditions close to those of the Pacific Ocean in the modern ocean (Peixoto and Oort, 1992) and minimum solar insolation wind stress from Glancy's (ms) GCM simulations. Simulations B, C, and D employed wind stress patterns from the same GCM study but with maximum rather than minimum solar insolation. Simulation B employed the same modern P–E boundary conditions used in simulation A. Simulation C used precipitation boundary conditions representative of moderate values from published Cretaceous GCM simulations (Barron and Washington, 1982), while simulation D employed the very highest precipitation values from the GCMs. Evaporation values for all simulations were kept at modern values (table 3).

The models were run for a total of 4 yrs of simulation time. Long model runs indicated that steady state was achieved in 3 to 4 yrs of simulation time. Only results from the fourth year of simulation are presented here. One year of model simulation took approx 16 hrs of CPU time on a Sun SPARC-20 workstation.

MODEL RESULTS

The four model runs produced a wealth of output, only a fraction of which can be presented here. The results presented below emphasize how differing wind and precipitation rates influence the salinity and oxygen within the seaway. Circulation in the seaway is examined within the context of standard principles of physical oceanography. Intense, short-term meteorological events (for example hurricanes) are not considered here, although they may have altered seaway hydrography on a short term basis (Eriksen and Slingerland, 1990; Jewell, 1993).

Circulation.—Subtidal velocity was calculated by averaging the velocity output over an M_2 tidal cycle (12.42 hrs). The results of model simulations A and B (both summer and winter) are presented below. In this manner, the differences between minimum and maximum solar insolation wind stress fields could be examined during seasonal extremes (fig. 3).

For simulation A in winter (minimum solar insolation winds), the circulation consists of an intense western boundary current and weak, broad eastern boundary current (fig. 4A). This pattern can be explained in terms of the vorticity balance between wind stress curl, the zonal gradient of the Coriolis force, and lateral friction. Similar analyses of ocean basins are described in several classic physical oceanography papers (Stommel, 1948; Reid, 1948; Munk, 1950). Minimum solar insolation winter winds have a negative wind stress curl which, although less intense than the average of the modern atmosphere, has the same general configuration (fig. 2). These winds impart negative vorticity to surface waters in a manner similar to that seen in subtropical gyres of the modern ocean. The negative vorticity caused by the wind field is balanced by the vorticity caused by lateral friction (positive along the

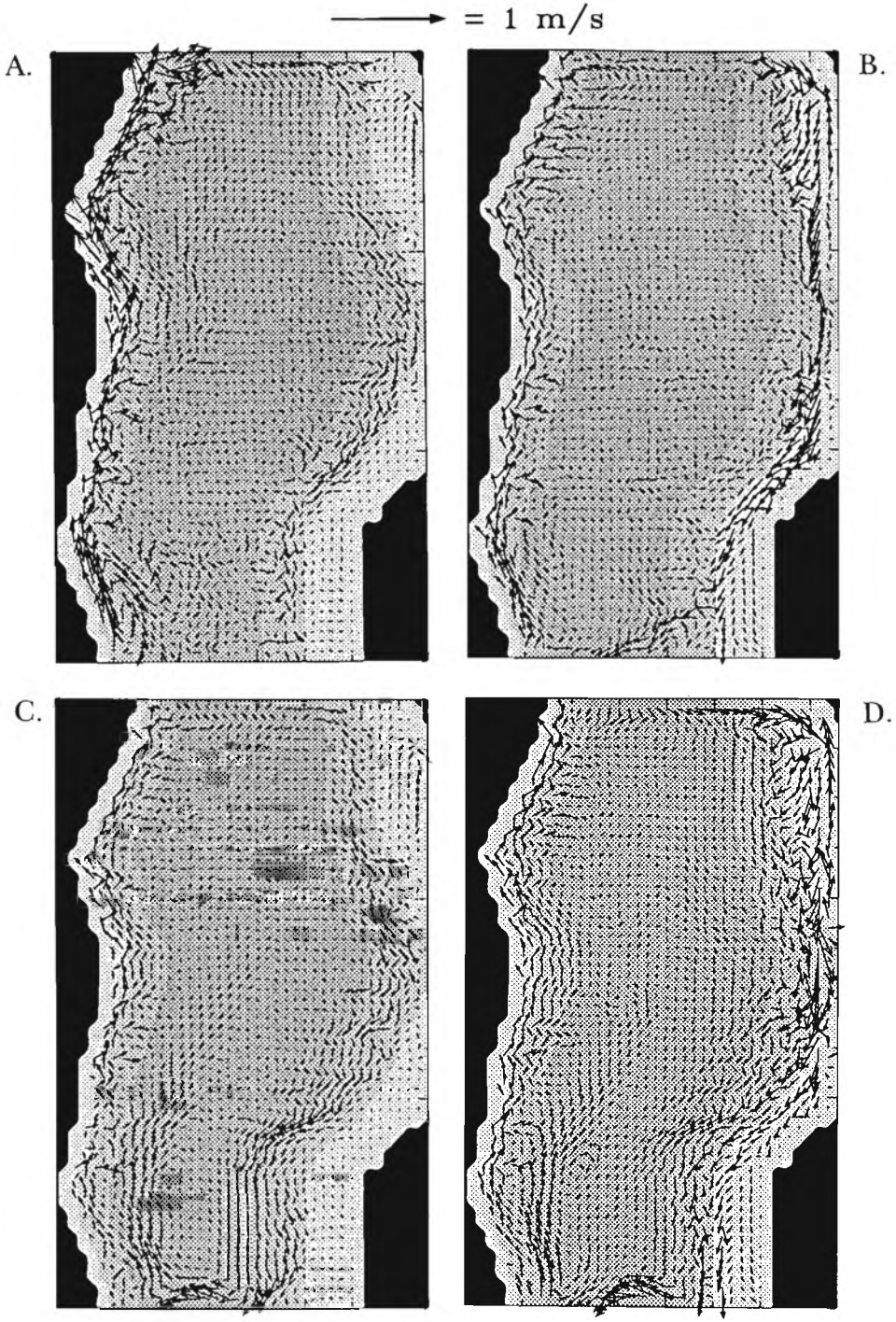

Fig. 4. Surface velocities averaged over an M_2 tidal cycle. Frames (A) to (D) correspond to figure 3A to D. (A) Minimum solar insolation winter surface velocity; (B) Minimum solar insolation summer surface velocity; (C) maximum solar insolation winter surface velocity; (D) maximum solar insolation summer surface velocity.

western boundary and negative along the eastern boundary) and the poleward increase in negative vorticity due to planetary rotation. Under these circumstances, an intense, narrow western boundary current and broad eastern boundary current is necessary to maintain the vorticity balance. These features are readily apparent in the minimum solar insolation, winter circulation of the seaway (fig. 4A), and they are also shown in the Cretaceous seaway simulations of Eriksen and Slingerland (1990, their fig. 6C).

The other three wind fields considered in this study (minimum insolation summer and maximum insolation summer and winter) have no obvious vorticity patterns (figs. 2; 3B, C, D). Under these situations, circulation is the result of vorticity due to lateral friction along the seaway boundaries being balanced by the northward increase in planetary vorticity. The seaway circulation thus nominally imitates the basin described by Fofonoff (1954) in which there is no wind stress curl, and the vorticity balance is composed only of lateral friction and planetary vorticity. At a given latitude, the Fofonoff model predicts that the western and eastern boundary currents will be of equal magnitude. This is clearly observed in the subtidal velocity fields of minimum insolation summer and maximum insolation summer and winter simulations (fig. 4B, C, D). The Fofonoff model also predicts intensification of the boundary currents to the north in response to increases in planetary vorticity. This feature is difficult to observe in the Cretaceous seaway simulations due to the irregular shorelines of the basin.

Average water mass flux and residence times (calculated as volume divided by mass flux) were calculated for the shallow and deep water (arbitrarily divided at 100 m depth) of all model runs (table 4). Shallow water residence times vary between 1 and 2 yrs for simulations A and B, whereas deep water residence times are somewhat longer (3-5 yrs). The moderate and high precipitation simulations have shallow and deep water residence times which are significantly shorter than the low precipitation simulations (table 4). These observations are clearly reflected in east-west cross sections of the north-south component of subtidal velocity (fig. 5). North-south subtidal velocity is < 10 cm/s at all depths in the low precipitation scenario (simulation B) (fig. 5A). Surface north-south veloc-

TABLE 4

Summary of water mass flux (in units of Sv = 10^6 m^3/s) and residence times (yrs) of the numerical simulations

Simulation	Season	Shallow Water (< 100 m) Mass Flux	Shallow Water Residence Time	Deep Water (> 100 m) Mass Flux	Deep Water Residence Time
A	winter	3.1	2.1	2.8	4.6
A	summer	2.6	2.5	2.3	5.5
B	winter	4.3	1.5	4.1	3.1
B	summer	5.8	1.1	5.5	2.3
C	winter	4.6	1.4	4.3	3.0
D	winter	11.0	0.6	10.2	1.3

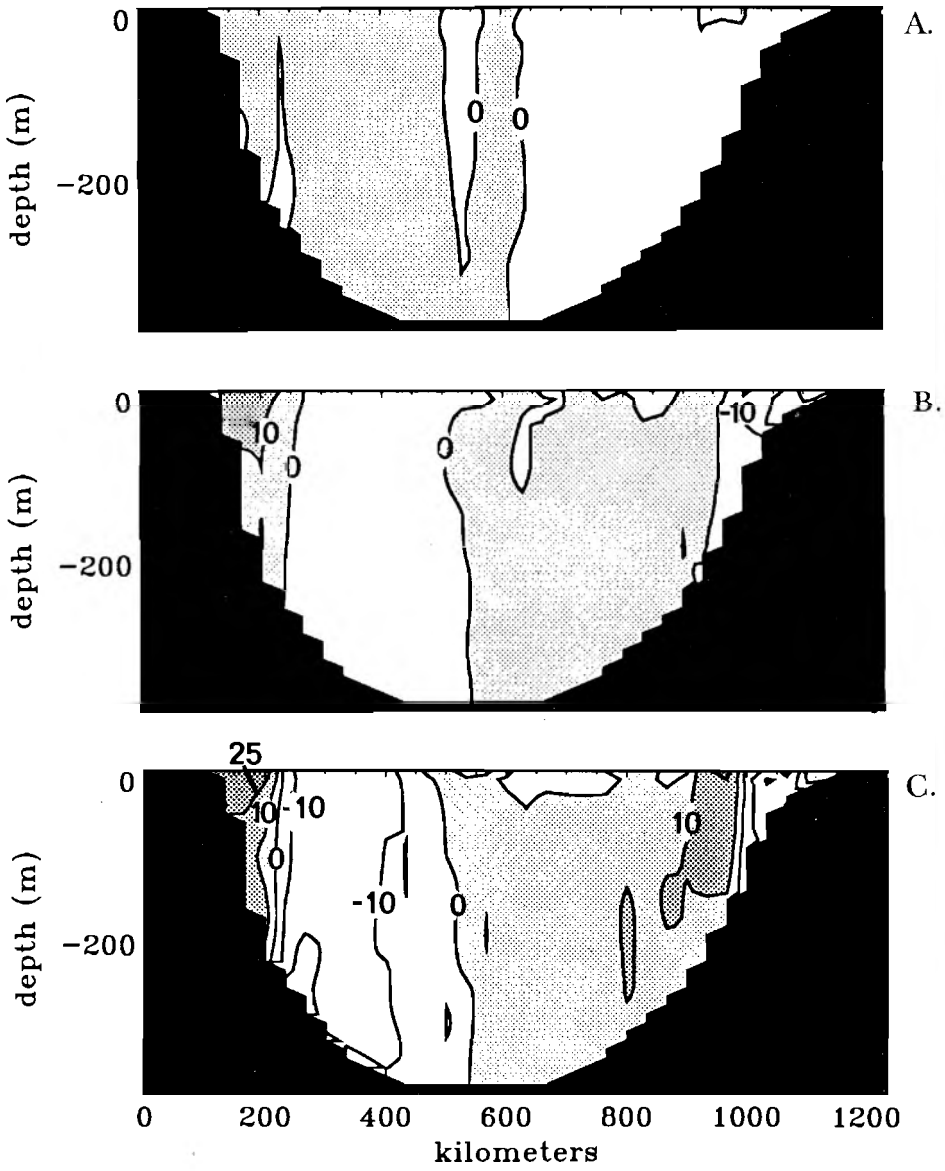

Fig. 5. Cross section of north-south velocity component averaged over an M_2 tidal cycle at paleolatitude of what is now northern Colorado and Nebraska (fig. 1) for winter maximum solar insolation. (A) Simulation B; (B) simulation C; (C) simulation D.

ity is >25 cm/s and deep water north-south velocity >10 cm/s in the high precipitation scenario (simulation D) (fig. 5C). These differences are believed to be a direct result of differing P–E input to the seaway and are discussed in more detail below.

In a modeling study of tropical storms in the Cretaceous North American seaway, Eriksen and Slingerland (1990) state that most sedimentological evidence suggests that circulation during these storms was cyclonic (counterclockwise). It should be emphasized that the mean, longterm anti-cyclonic circulation shown in this study would typically not leave significant sedimentological evidence in the geologic record.

Salinity.—Surface salinity results are presented for the winter of all four simulations (table 3). Comparison of results for simulations A and B allow examination of the effect that a relatively strong western boundary current has on surface salinity. When this boundary current is present, a tongue of high salinity (35.5-36.0 ppt) water is swept northward in the western portion of the domain (fig. 6A). When the eastern and western boundary currents are of approximately equal magnitude (simulation B), the high salinity tongue is found in the central portion of the domain where circulation is relatively stagnant (fig. 6B).

Increasing precipitation to 2.0 m/yr (table 3, simulation C) produces surface salinities considerably fresher than those of simulations A or B (fig. 6C). A broad zone of relatively low salinity water (<33.0 ppt) is formed in the central portion of the seaway. This is also an area of relatively stagnant surface water flow (fig. 4C, D) which allows the influence of enhanced precipitation to become more noticeable. Surface salinity is somewhat higher (33.0-34.0 ppt) in the western portion of the seaway despite significant freshwater input from river inflow of the Cordilleran highlands to the west.

The very highest precipitation simulations (4.0 m/yr; simulation D) produce the same pattern of horizontal salinity gradients as simulation C, although the absolute salinity values are ~3-4 ppt lower (fig. 6D). Surface salinity as low as 29 ppt occurs in the northeastern portion of the seaway. Small irregularities in salinity along the western boundary reflect the influence of river inflow, although as with simulation C, the effect on surface salinity is not very pronounced.

Salinity cross sections show the nature of vertical salinity stratification for simulations C and D (figs. 7, 8). The very lowest salinity water is restricted to the uppermost 20 m of the water column. The stronger winds of storms would no doubt result in more thorough mixing of salinity on a temporary basis (Jewell, 1993). In general, isohalines extend to greater depths in the western portion of the seaway than in the east (figs. 7, 8). This may be the result of river input on the western edge of the domain which, while not causing significantly lower surface water salinity (fig. 6C, D), results in somewhat less salty water throughout the upper 100 m of the water column.

An important relationship can be observed between vertical salinity gradients, surface water elevation, and circulation in the seaway. The

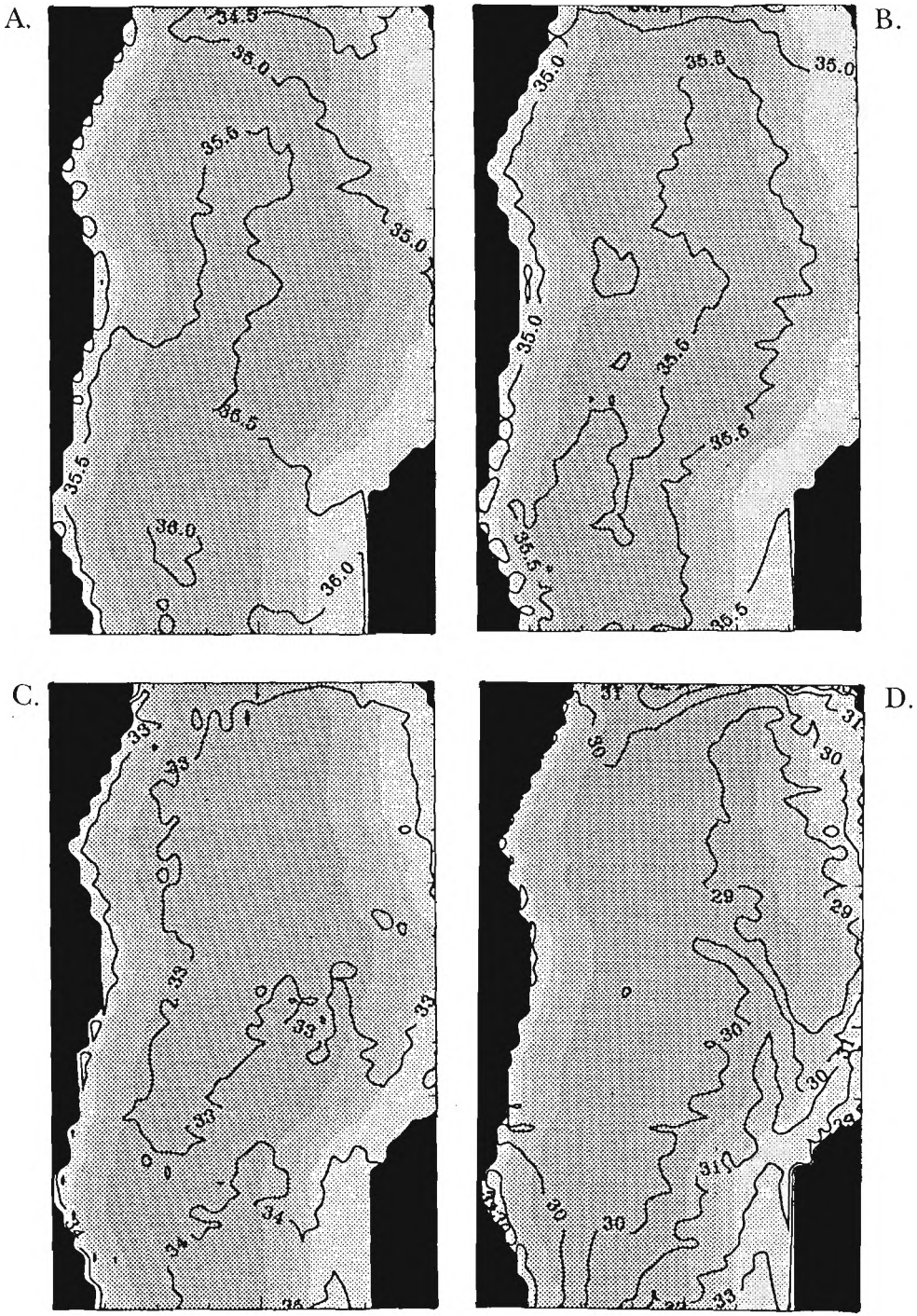

Fig. 6. Sea surface salinity. (A) Simulation A; (B) simulation B; (C) simulation C; (D) simulation D. Contour interval is 0.5 ppt in (A) and (B) and 1.0 ppt in (C) and (D) (see table 2).

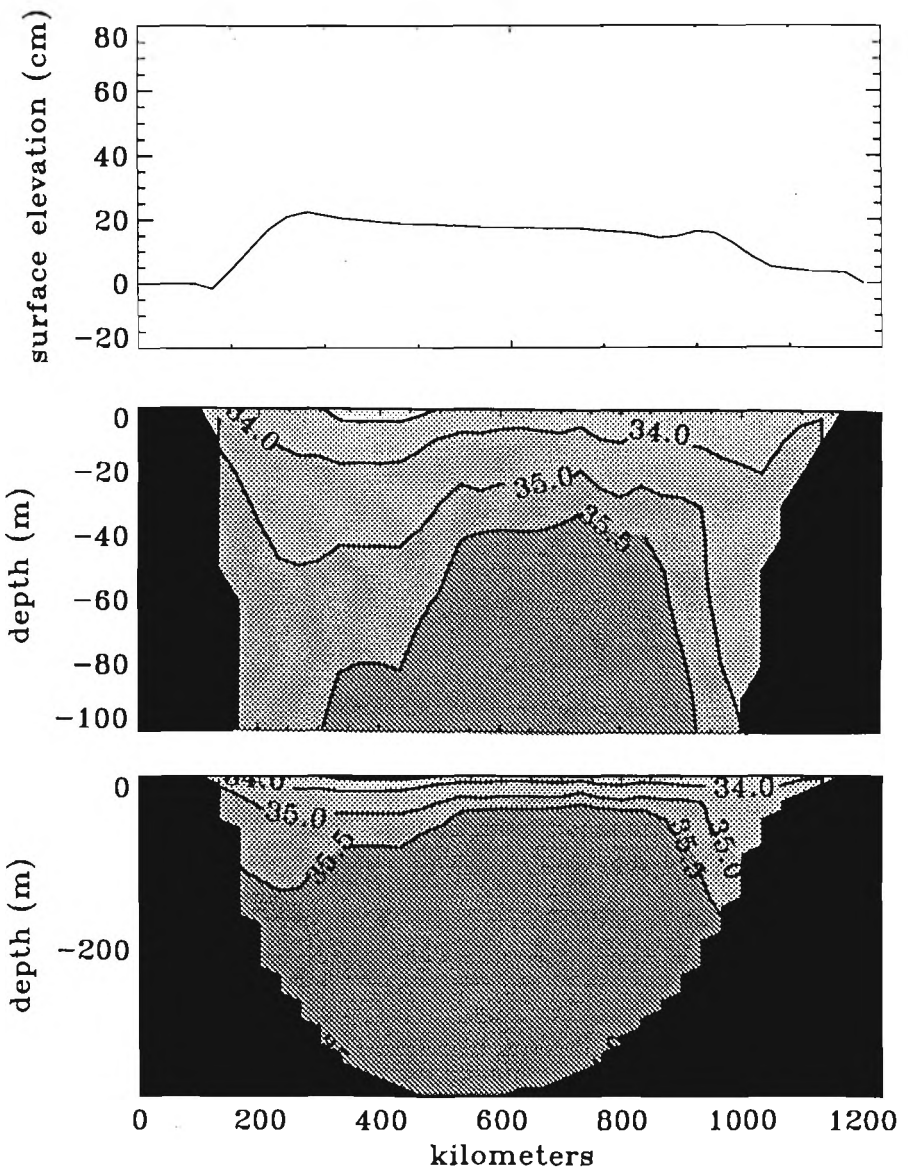

Fig. 7. Cross section of surface elevation and salinity for moderate P–E simulation (simulation C) at approximate paleolatitude of northern Colorado and Nebraska (fig. 1).

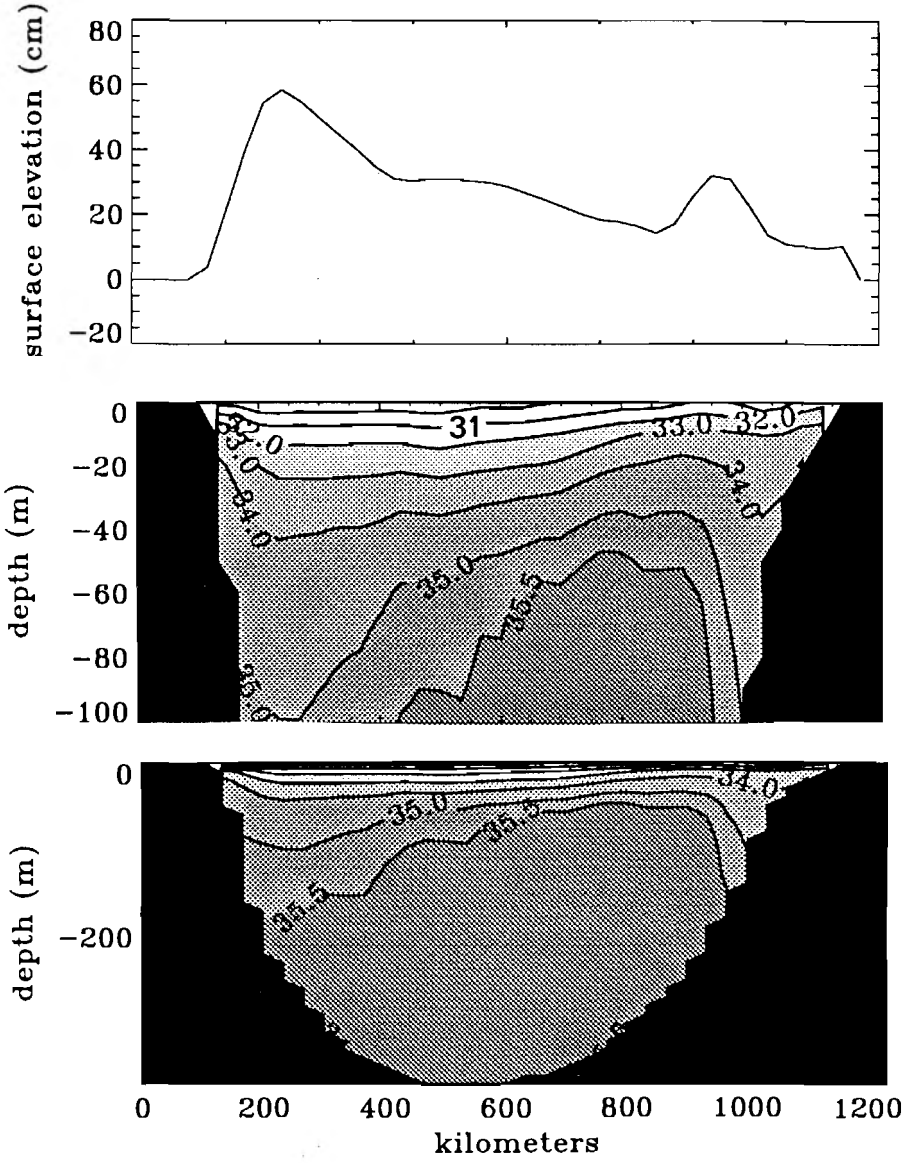

Fig. 8. Cross section of surface elevation and salinity for high P–E simulation (simulation D) at approximate paleolatitude of northern Colorado and Nebraska (fig. 1).

relatively low salinity in the upper 100 m of the western portion of the seaway results in a pronounced surface water elevation gradient in this area (figs. 7, 8). Circulation in the seaway intensifies as a result of these surface pressure gradients. The result is vigorous circulation and relatively short residence times for both shallow and deep water for the highest P–E simulation (table 4).

Oxygen.—Results of dissolved oxygen simulations are presented as "apparent oxygen utilization" (AOU) (defined as AOU = calculated oxygen saturation concentrations minus observed oxygen concentration). AOU has the advantage of representing the amount of oxygen consumed as the result of biogeochemical processes without considering the influence that temperature and salinity have on oxygen concentrations.

As with salinity, AOU stabilized after 3 or 4 yrs of simulation time. Maximum AOU is modest (<20 μmol/L) in all simulations (fig. 9). Virtually no oxygen utilization is observed above 200 m. In general, AOU is somewhat higher in the western portion of the domain than in the eastern portion. An interesting feature of the oxygen simulations is that maximum deep water AOU decreases as the degree of vertical salinity stratification increases. The simulation that produces the lowest surface salinity (simulation D) has the smallest (<10 μmol/L) AOU (fig. 9C). These observations can be explained within the context of the circulation and deep water residence times discussed previously. Deep water mass flux increases in response to the greater horizontal salinity and surface water elevation gradients (figs. 7, 8). Deep water residence time and hence AOU both decrease as P–E increases. The importance of these observations to the maintenance of anoxia in the seaway as well as to global anoxic events is discussed below.

DISCUSSION

*Surface salinity and the role of rivers.*Considerable speculation exists about the role that rivers played in seaway hydrography (Pratt, 1984; Arthur and others, 1985; Hay, Eicher, and Diner, 1993; Glancy and others, 1993). In all the simulations of this study, the influence of freshwater from rivers of the western Cordilleran mountains is very subtle. At the water surface, freshwater discharge appears to be masked by northward advection of high salinity water by western boundary currents which bring salty water northward from the Gulf of Mexico. These currents are present in all the simulations (fig. 6) and, as explained above, are a direct result of the vorticity balance in the seaway. Freshwater from the western highlands does appear to be manifested as a lens of relatively low salinity water in the upper 100 m of the water column in high precipitation scenarios, however (figs. 7, 8).

Total river mass flux for the seaway simulations can be estimated by summing the P–E values for the western boundary grid points of the model. For the modest P–E scenario (simulation C), total river discharge is $\sim 12{,}000$ m^3/s (or 0.012 Sv where 1 Sv = 10^6 m^3/s) while for the high P–E scenario (simulation D), it is 24,000 m^3/s (0.024 Sv). Both the these

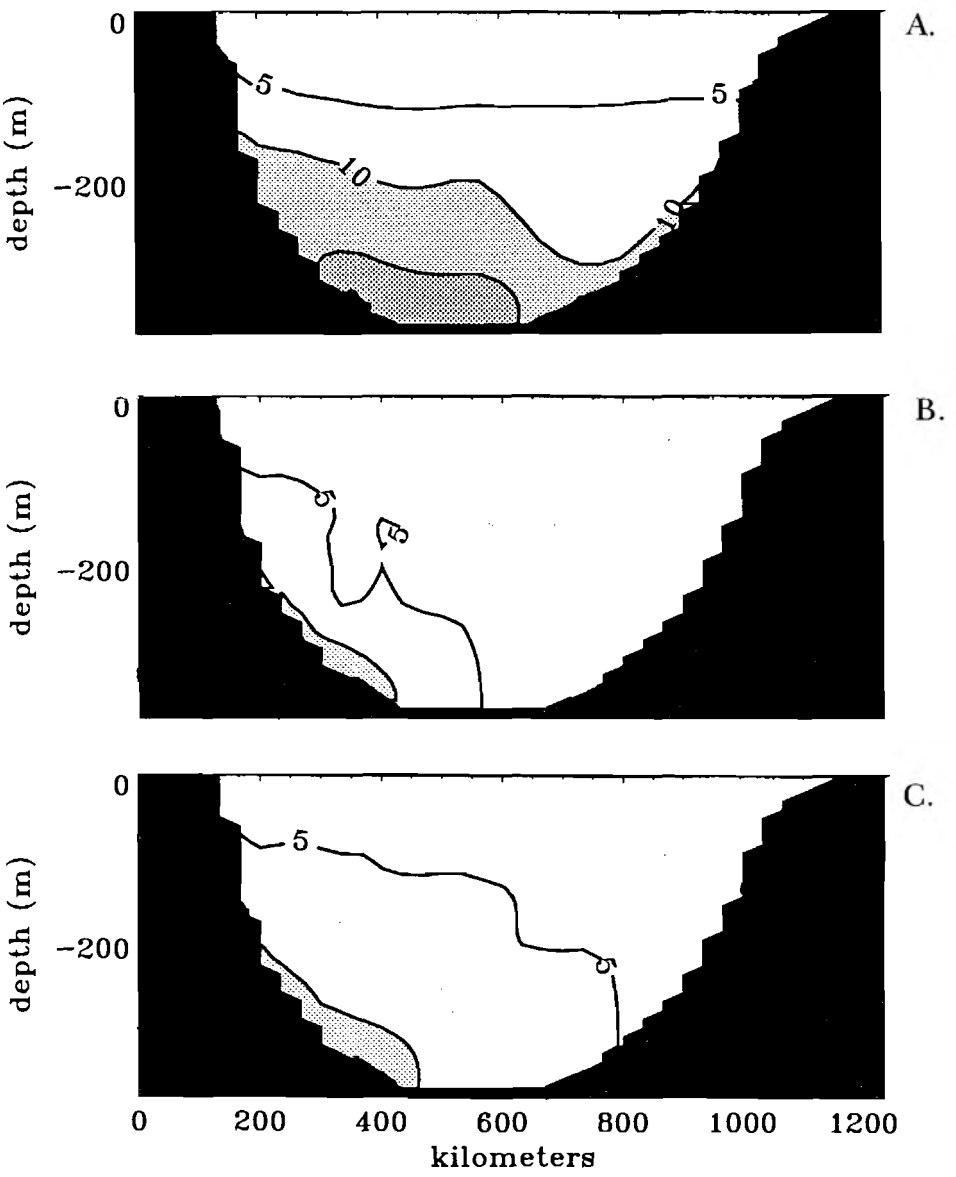

Fig. 9. Cross section of apparent oxygen utilization (AOU) at paleolatitude of approx 45°N (fig. 1). Contours are in units of 5 μmol/L. (A) simulation B; (B) simulation C; (C) simulation D.

mass flux rates are considerably less than calculated shallow water mass flux for the seaway as a whole (table 4). It is, therefore, not surprising that a significant freshwater river signal is not observed along the western boundary of the seaway.

The modeling procedure of representing a river as relatively small discharge at every model grid point rather than larger outflow at a smaller number of grid points represents a potential source of model error. Modeling river flow in this manner is justified by considering the geometry of river basins in the Sevier highlands to the west and by examining data from modern river basins.

Paleogeographic reconstructions from the Cenomanian-Turonian suggest that the Sevier orogenic belt occupied a relative narrow (300-500 km wide) band of emergent land to the west of the seaway (Funnel, 1990; Eaton and Nations, 1991). If approximately half this land was draining into the seaway, then the total drainage area encompassed by this model would be 0.44×10^6 km^2. This is a significantly smaller drainage area than many of the river basins found in high precipitation areas of the modern world (table 5). The long, linear shape of the Sevier highlands probably resulted in a number of relatively small river drainage basins. If so, then the water discharge rate from individual rivers was probably significantly less than the maximum freshwater discharge of 24,000 m^3/s (0.024 Sv or 733 km^3/yr). Discharges of this magnitude are within the range of modern tropical latitude rivers such as the Mekong and Irrawady Rivers (table 5). In general, freshwater plumes from rivers of this size do not extend for significant distances into the adjacent ocean. The Amazon River is volumetrically the largest river in the world (approximate average discharge of 100,000 m^3/s), and low salinity lenses from the Amazon plume extend far into the open Atlantic Ocean (Ryther, Menzel, and Corwin, 1967). However, discharge from the Amazon is probably several times greater than discharge from *all* the rivers draining into the Cretaceous North American Interior seaway. It is therefore not surpris-

TABLE 5

Summary of drainage basin area and river discharge rates for selected modern river basins (from Milliman and Meade, 1983) and the proposed rates for the Cretaceous Interior Seaway

River (country)	Drainage Area (10^6 km^2)	River Discharge (km^3 yr^{-1})
Amazon (Brazil)	6.15	6300
Orinoco (Venezuala)	0.99	1100
Mekong (Vietnam)	0.79	470
Irrawady (Burma)	0.43	428
Indus (Pakistan)	0.97	238
Cretaceous, Simulation C	~0.44	~367*
Cretaceous, Simulation D	~0.44	~733*

* Sum of all rivers within the model domain.

ing that these rivers do not play a prominent role in numerical simulations of the seaway salinity.

The fact that river runoff appears to have had little effect on the overall surface salinity of the seaway does not necessarily contradict observations that the type of sediment delivered to the seaway bottom was significantly different between periods of high and low precipitation in the seaway (Pratt, 1984). Even small and moderate sized modern rivers are capable of delivering significant suspended sediment to continental margins. Sediment delivery from small rivers is particularly high in tectonically active, tropical environments of the modern world (Milliman and Meade, 1983), and a similar effect would logically be expected in the Cretaceous seaway. As shown in this study, higher precipitation tends to increase the intensity of overall circulation in the seaway (table 4), and hence it would be logical to expect that sedimentation patterns would likewise be different for high and low precipitation scenarios.

Controls of deep water oxygen.—The relatively low model AOU simulated in the deep waters of the Cretaceous Interior seaway can be explained within the context of simple mass balance calculations of oxygen and circulation. Water will become anoxic when the sinks of oxygen (that is oxygen demand) exceed oxygen sources in the bottom water. Oxygen sources and sinks can be considered by the ratio, R.

$$R = \frac{O_{2\text{sink}}}{O_{2\text{source}}} \tag{11}$$

When $R < 1$, the water is at least partially oxygenated. When $R > 1$, then the water becomes anoxic.

As an initial simplification for understanding bottom water anoxia, the vertical mixing of oxygen from the surface will not be considered. The primary source of oxygen in bottom waters is thus horizontal advective or diffusive transport from outside the basin, that is oxygen flux in = (oxygen concentration) × (mass flux). Mass flux in or out of the seaway bottom waters would be net velocity across the seaway boundaries multiplied by the seaway cross-sectional area.

The primary sink for oxygen in the bottom water is decay of organic matter settling downward from the photic zone. The net oxygen sink would simply be: oxygen flux out = (organic oxidation rate) × (surface area). This expression can be recast in terms of carbon flux to the bottom waters by simply multiplying by the appropriate carbon:oxygen molar conversion factor.

The sources and sinks of oxygen now allow (11) to be rewritten as:

$$R = \frac{O_{2\text{surface demand}} \cdot \text{surface area}}{O_{2\text{in}} \cdot \text{water mass flux}}$$

Many processes in marine basins can be considered in terms of residence time that is, basin volume divided by mass flux in or out of the basin. Water residence time, τ, is defined as:

$$\tau = \frac{\text{water mass flux}}{\text{water volume}}$$

This deep water residence time can also be derived by multiplying the numerator and denominator of this expression by depth. Doing this in conjunction with appropriate conversion factors produces the relationships:

$$R = \frac{O_{2\text{surface demand}} \cdot \text{surface area}}{O_{2\text{in}} \cdot \text{water mass flux}} \cdot \frac{\text{depth}}{\text{depth}}$$

$$= \frac{O_{2\text{surface demand}} \cdot \text{volume}}{O_{2\text{in}} \cdot \text{mass flux} \cdot \text{depth}}$$

$$= \frac{O_{2\text{surface demand}} \cdot \text{water residence time}}{O_{2\text{in}} \cdot \text{depth}}$$

This final expression allows development of anoxia to be considered in terms of three simple factors: surface oxygen demand, depth, and residence time. Data for these three factors have been assembled for six modern marine basin (fig. 10; table 6). For all basins except the Baltic Sea, the depth of the bottom water layer is the average basin depth minus 100 m (the presumed thickness of the surface layer). For the relatively shallow Baltic Sea, the surface layer is assumed to be 50 m. Data on surface productivity (expressed as gC m^{-2}/yr) is much more common than data on carbon flux (that is, oxygen demand) to bottom waters. For the purpose of this analysis, carbon flux is assumed to be 20 percent of surface productivity. This value is typical of fluxes below 100 m depth (Bishop, 1989).

In all cases, the simple mass balance calculations presented above correctly forecast whether a modern marginal basin will be oxic or anoxic (fig. 10). Several points relevant to the Cretaceous Interior Seaway can be gleaned from this analysis. Bottom water anoxia can develop in relatively shallow basins (<500 m deep) with relatively short deep water residence times and modest surface productivity (for example the Baltic Sea). Shallow basins have relatively small volumes of deep water and hence limited "oxygen inertia," that is, the ability to oxidize organic matter that sinks from the photic zone. In this sense, relatively shallow basins such as the Cretaceous Interior seaway bear a closer resemblance to the Baltic Sea than to deep, long residence time basins such as the Black Sea. Understanding the deep water residence time of the seaway is thus critical to predicting the development of anoxia within the basin. Significantly higher productivity such as that observed in upwelling situations (the order of 1000 gC m^{-2}/yr) could also lead to anoxia (fig. 10). For the Cenomanian-Turonian period, however, such high productivities are considered unlikely (Pratt, 1985).

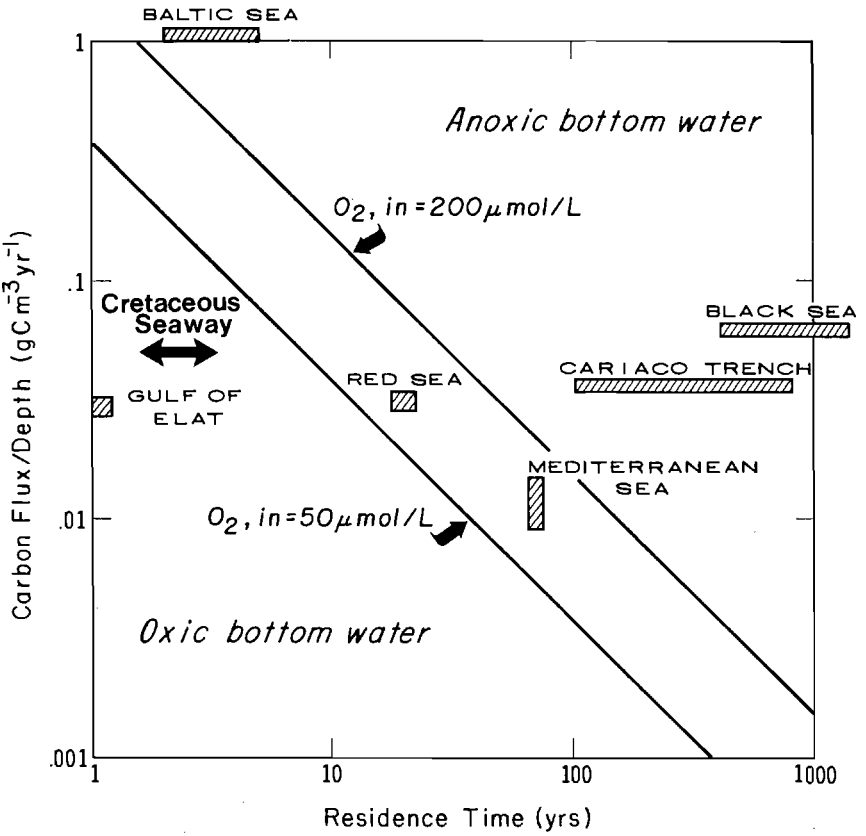

Fig. 10. Values of surface productivity, depth, and residence time for a number of modern borderland basins. (Carbon flux to the deep water of the basin is assumed to be 20 percent of surface productivity.)

The relatively low AOU concentrations (<20 μmol/L) calculated for all Cretaceous seaway model runs are a direct consequence of the magnitude of deep water exchange in the seaway with the open ocean and the relatively short residence time of deep water in the seaway (table 4). As shown in previous simulations (Jewell, 1993), even modest vertical salinity gradients (>2 ppt) are capable of preventing significant downward mixing of oxygenated surface waters. On the other hand, extremely high freshwater input to the seaway surface will cause significant horizontal salinity gradients (fig. 6C, 6D). Such gradients are likely to form whether the freshwater enters the seaway from the Arctic Ocean (Hay, Eicher, and Diner, 1993), as river inflow from the west, or (as in this case of these simulations) as uniform precipitation throughout the seaway. As demonstrated in this study, horizontal salinity gradients set up horizontal

TABLE 6

Summary of depth, residence time, and carbon flux data for enclosed marine basins of the modern ocean

Basin	Average Depth (m)	Residence Time (yrs)	Organic Carbon Flux (gC m^{-2}/yr)
Mediterranean	1400*	70**	10–20***#
Black Sea	1200##	400–200###	72§
Baltic Sea	65§§	2–5§§§	20+#
Cariaco Trench	~1000++	100–800+++	35++#
Red Sea	490&	22&	12&&#
Gulf of Elat	~1000&&&	~1&&&	32$#

* Hopkins (1978); ** Pickard and Emery (1983); *** Berger and others (1987); # calculated as 20 percent of primary productivity; ## Ross and others (1974); ### Murray (1991); § Lein and Ivanov (1991); §§ Winterhalter (1981); §§§ Kullenberg (1981); + Halfors and others (1981); ++ depth below sill; Richards and Vaccaro (1956); +++ Fanning and Pilson; Dueser (1973); & Morcos (1970); && Weikert (1987); &&& approximated from Klinker and others (1976); $ Levanon-Spanier, Padan, and Reiss (1979).

pressure gradients which in turn increase the circulation of both surface and deep waters. The result is decreasing deep water residence times and AOU (table 4, fig. 9).

The relatively short deep water residence times in these simulations are at least in part the result of not having a sill at the southern entrance to the seaway model domain. The existence of such a sill has been suggested by research on the Albian seaway (Kaufmann, 1984; Winker and Buffler, 1989), although its existence during the Cenomanian-Turonian is debatable. If such a sill were to result in much greater deep water residence time in the seaway, then the mass balance calculations presented above suggest that deep water anoxic conditions would have prevailed regardless of oxygen concentrations of water entering the seaway (fig. 10). If a sill did not exist and if the residence time of deep water in the seaway was relatively short (the order of several yrs) then anoxia in the seaway was almost certainly the result of anoxic or suboxic water entering from the open ocean. The existence and depth of a sill at the seaway entrance is therefore a critical issue for determining the controls of anoxia in the Cretaceous seaway.

CONCLUSIONS

Three-dimensional hydrodynamic simulations of salinity and oxygen of the transgressive Cenomanian-Turonian period of the Cretaceous North American seaway provide insight into several long-standing issues regarding this unique geologic setting.

1. Surface water circulation in the seaway between paleolatitudes of approx 30°N and 50°N was dominated by a subtropical gyre. The relative

strength of western and eastern boundary currents depended on the zonal wind stress curl and wind magnitude which in turn appears to have been related to the amount of solar insolation. The residence time of surface water in the seaway is calculated to be between 0.6 and 2.5 yrs with the shortest residence times being the result of surface water pressure gradients set up by high precipitation. Surface water residence times in the subtropical gyre of the three dimensional seaway simulations are considerably shorter than residence times calculated directly from the wind stress curl via the Sverdrup equation (Jewell, 1993).

2. Surface salinity effects of river inflow from the Sevier orogenic belt to the west are generally masked by the strong northward flowing western boundary current. The relatively small drainage basin area of the Sevier orogenic belt precludes formation of large rivers with sufficient freshwater volume flux to make a significant impact on the salinity of the strong boundary current. Surface salinity in the seaway is largely a function of the intensity of the subtropical gyre, with the largest freshwater signal being seen in the central portions of the seaway where circulation is weakest or in the northeast portion of the domain where surface water residence time is greatest.

3. Very high P–E rates ($\sim$3.5 m/yr) are necessary to produce the 20 percent freshwater dilutions suggested by the oxygen isotope records of pelagic carbonates from the seaway. This is considerably higher than the P–E rates suggested by Jewell (1993) for similar freshwater dilutions. The short surface water residence times of these simulations presented here account for the differences between these two modeling studies.

4. Apparent oxygen utilization (AOU) is low ($<$20 μmol/L) for all simulations. Higher surface salinity gradients produce higher surface water elevation gradients and hence, more vigorous deep water exchange and lower AOU in the deeper portions of the seaway. Simple mass balance calculations show that low AOU values are the result of high deep water exchange rates through the open boundaries and relatively low deep water residence times. Restricted circulation of the deep water due to the existence of a sill at the seaway entrance or higher surface productivity would produce higher AOU. If the seaway experienced significant deep water exchange with the open ocean, then the well-documented anoxia in the seaway was probably the result of disoxic or anoxic water from the oxygen-minimum zone of the open ocean and was possibly associated with the Cenomain-Turonian global anoxic event.

ACKNOWLEDGMENTS

Tom Glancy provided data from his Ph.D. thesis. Acknowledgment is made to the Donors of the Petroleum Research Fund, administered by the American Chemical Society for support of this research.

References

Arthur, M. A., Dean, W. E., Pollastro, R. M., Claypool, G. E. Scholle, P. A., and Claypool, G. E., 1985, Comparative geochemical and mineralogical studies of two cyclic transgressive pelagic limestone units, Cretaceous Western Interior Basin, U. S., *in* Pratt, L. M., Kauffman, E. G., and Zelt, F. B., editors, Fine-grained deposits and biofacies of the Cretaceous Western Interior Seaway: Evidence for cyclic processes: Society of Economic Paleontologists and Mineralogists, Field Trip Guidebook 4, p. 16–27.

American Society of Civil Engineers, Task Committee on Turbulence Models in Hydraulic Computations, 1988, Turbulence modeling of surface water flow and transport: Part III: Journal of Hydraulic Engineering, v. 114, p. 1015–1033.

Barron, E. J., Arthur, M. A., and Kauffman, E. J., 1985, Cretaceous rhythmic bedding sequences: a plausible link between orbital variations and climate: Earth and Planetary Science Letters, v. 72, p. 327–340.

Barron, E. J., and Peterson, W. H., 1990, Mid-Cretaceous ocean circulation: results from model sensitivity studies: Paleoceanography, v. 5, p. 319–337.

Barron, E. J., and Washington, W. M., 1982, Cretaceous climate: a comparison of atmospheric simulations with the geologic record: Palaeogeography, Palaeoclimatology, and Palaeoecology, v. 40, p. 103–133.

Batteen, M. L., and Han, Y.-J., 1981, On the computational noise of finite-difference schemes used in ocean models: Tellus, v. 33, p. 387–396.

Berger, W. H., Smetacek, V. S., and Wefer, G. 1989, Ocean productivity and paleoproductivity—an overview, *in* Berger, W. H., and others, editors., Productivity in the Ocean: Past and Present, New York, John Wiley, p. 1–34.

Bishop, J. K. B., 1989, Regional extremes in particulate matter composition and flux: effects on the chemistry of the ocean interior, *in* Berger, W. H., and other editors. Productivity in the Ocean: Past and Present, New York, John Wiley, p. 117–137.

Blumberg, A. F., and G. L. Mellor, 1987, A description of a three-dimensional coastal ocean circulation model, *in* Heaps, N. S., editor, Three dimensional coastal circulation ocean models, American Geophysical Union Coastal and Estuarine Sciences Series, v. 4, p. 1–16.

Bralower, T. J., and Theirstein, H. R., 1984, Low Productivity and slow deep-water circulation in Mid-Cretaceous oceans: Geology, v. 12, p. 614–618.

Budyko, M. I., 1986, The evolution of the biosphere: Dordrecht, Reidel, 423 p.

Carpenter, J. H., 1966, New measurements of oxygen solubility in pure and natural water: Limnology and oceanography, v. 11, p. 264–277.

Conner, W. P., 1991, A users manual for the Princeton numerical ocean model: Stennis Space Center Institute of Naval Oceanography Special Report 5, Mississippi, 69 p.

Deuser, W. G., 1973, Cariaco Trench: oxidation of organic matter and residence time of anoxic water: Nature, v. 242, p. 601–603.

Eaton, J. G., and Nations, J. D., 1991, Introduction; Tectonic setting along the margin of the Cretaceous Western Interior Seaway, southwestern Utah and Arizona, *in* Nations, J. D., and Eaton, J. G., editors, Stratigraphy, depositional environments, and sedimentary tectonics of the western margin, Cretaceous Western Interior Seaway: Geological Society of America Special Paper 260, p. 1–8.

Eicher, D. L., and Diner, R., 1985, Foraminifera as indicators of water mass in the Cretaceous Greenhorn Sea, Western Interior, *in* Pratt, L. M., Kauffman, E. G., and Zelt, F. B., editors, Fine-grained deposits and biofacies of the Cretaceous Western Interior Seaway: Evidence for cyclic processes: Society of Economic Paleontologists and Mineralogists, Field Trip Guidebook 4, p. 60–71.

Emerson, S., and Hedges, J. I., 1988, Processes controlling the organic carbon content of the open ocean: Paleoceanography, v. 3, p. 621–634.

Ericksen, M. C., and Slingerland, R. L., 1990, Numerical simulations of tidal and wind-driven circulation in the Cretaceous Interior Seaway of North America: Geological Society of America Bulletin, v. 102, p. 1499–1516.

Ezer, T., and Mellor, G. L., 1992, A numerical study of the variability and separation of the Gulf Stream induced by surface atmospheric forcing and lateral boundary forces: Journal of Physical Oceanography, v. 22, p. 660–682.

Fanning, K. A., and Pilson, M. E. Q., 1972, A model for the anoxic zone in the Cariaco Trench: Deep Sea Research, v. 19, p. 847–863.

Fisher, C. G., Hay, W. W., and Eicher, D. L., 1994, Oceanic front in the Greenhorn Sea (late middle through late Cenomanian): Paleoceanography, v. 9, p. 879–892.

Fofonoff, N. P., 1954, Steady flow in a frictionless homogeneous ocean: Journal of Marine Research, v. 13, p. 254–262.
Funnel, B. M., 1990, Global and European Cretaceous shorelines, stage by stage, *in* Ginsberg, R. N. and Beaudoin, B., Cretaceous resources, events, and rhythms: background and plans for research, NATO-ASI series, p. 197–202.
Galperin, B., and Mellor, G. L., 1990, A time-dependent, three-dimensional model of the Delaware Bay and River system: Part 1: Description of the model and tidal analysis: Estuarine, Coastal, and Shelf Science, v. 31, p. 231–281.
Glancy, T. J., ms, 1992, Sensitivity of modeled Cretaceous climate to insolation forcing created by varying earth-sun orbital relationships: Ph.D. thesis, University of Rhode Island, Kingston, Rhode Island, 735 p.
Glancy, T. J., Arthur, M. A., Barron, E. J., and Kaufmann, E. G., 1993, A paleoclimate model for the North American Cretaceous (Cenomanian-Turonian) epicontinental sea, *in* Caldwell, W. G. E. and Kaufmann, E. G., editors, Evolution of the Western Interior Seaway: Geological Association of Canada Special Paper 39, p. 219–242.
Graber, H. C., Beardsley, R. C., and Grant, W. D., 1989, Storm-generated surface waves and sediment resuspension in the East China and Yellow Seas: Journal of Physical Oceanography, v. 19, p. 1039–1059.
Haidvogel, D. B., Bryan, F. O., 1993, Ocean general circulation modeling, *in* Trenberth, K. E., editor, Climate System Modeling: Cambridge University Press, p. 317–412.
Halfors, G., Hiemi, A., Ackefors, H., Lassig, J., Leppakoski, E., 1981, Biological oceanography, *in* Voipo, A., editor, The Baltic Sea: Elsevier Oceanography Series 30, p. 219–274.
Hakkinen, S., and Mellor, G. L., 1990, One hundred years of Arctic ice cover variations as simulated by a one-dimensional, ice-ocean model, Journal of Geophysical Research, v. 95, p. 15,959–15,969.
Hancock, J. M., and Kauffman, E. G., 1979, The great transgressions of the Cretaceous: Journal of the Geological Society of London, v. 136, p. 175–186.
Hellerman, S., and Rosenstein, M., 1983, Normal monthly wind stress over the world ocean with error estimates: Journal of Physical Oceanography, v. 13, p. 1093–1104.
Hay, W. W., Eicher, D. L., and Diner, R., 1993, Physical oceanography and water masses in the Cretaceous Interior Seaway, *in* Caldwell, W. G. E. and Kaufmann, E. G., editors, Evolution of the Western Interior Seaway: Geological Association of Canada Special Paper 39, p. 297–318.
Hofmann, E. E., 1988, Plankton dynamics on the outer southeastern U.S. continental shelf. Part III: A couple physical biological model: Journal of Marine Research, v. 46, p. 919–946.
Holland, H. D., 1978, The chemistry of the atmosphere and oceans: New York, Wiley, 351 p.
Hopkins, T. S., 1978, Physical processes in the Mediterranean Basins, *in* Kjerfve, B., editor, Estuarine Transport Processes: Columbia, University of South Carolina Press, p. 269–310.
Jewell, P. W., 1992, Hydrodynamic controls of anoxia in shallow lakes in Whelan, J. K., and Farrington, J. W., editors, Organic matter: Productivity, accumulation, and preservation in recent and ancient sediments: New York, Columbia University Press, p. 201–228.
———— 1993, Water column stability, residence times, and anoxia in the Cretaceous North American seaway: Geology, v. 21, p. 579–582.
Jewell, P. W., Stallard, R. F., and Mellor, G. L., 1993, Numerical models of bottom shear stress and sediment distribution on the Amazon continental shelf: Journal of Sedimentary Petrology, v. 63, p. 734–745.
Kantha, L. H., Blumberg, A. F., and Mellor, G. L., 1990, Computing phase speeds at open boundary, Journal of Hydraulic Engineering, v. 116, p. 592–597.
Kauffman, E. G., 1984, Paleobiogeography and evolutionary response dynamics in the Cretaceous Western Interior Seaway of North America, *in* Westermann, G. E. G., editor, Jurassic-Cretaceous biochronology and paleogeography of North America: Geological Association of Canada Special Paper 27, p. 273–306.
Klinker, J., Reiss, Z., Kropach, I., Harpez, H., and Halicz, E., 1976, Observations on the circulation pattern in the Gulf of Elat (Aqaba), Red Sea: Isreal Journal of Earth Sciences, v. 25, p. 85–103.
Kominz, M., 1984, Oceanic ridge volumes and sea level change—an error analysis, in Schlee, J. S., editor, Interregional unconformities and hydrocarbon accumulation: American Association of Petroleum Geologists Memoir 36, p. 109–127.
Kullenberg, G., 1981, Physical oceanography, *in* Voipo, A., editor, The Baltic Sea: Elsevier Oceanography Series 30, p. 135–181.

Large, W. G., and Pond, S., 1981, Open ocean momentum flux measurements in moderate to strong winds, Journal of Physical Oceanography, v. 11, 324–336.
Lein, A. Y., and Ivanov, M. V., 1991, On the sulfur and carbon balances in the Black Sea, *in* Izdar, E., and Murray, J. W., editor, Black Sea oceanography: NATO Advanced Science Institutes Series C, Mathematical and Physical Sciences, v. 351, p. 307–318.
Levanon-Spanier, I., Padan, E., and Reiss, Z., 1979, Primary production in a desert-enclosed sea—the Gulf of Elat (Aqaba), Red Sea: Deep Sea Research, v. 26A, p. 673–685.
Levitus, S., 1982, Climatological atlas of the world ocean: National Oceanic and Atmospheric Administration Professional Paper 13, 173 p.
Mellor, G. L., and Ezer, T., 1991, A Gulf Stream model and an altimetry assimilation scheme: Journal of Geophysical Research, v. 96, p. 8779–8795.
Mellor, G. L., and Kantha, L., 1989, An ice-ocean model: Journal of Geophysical Research, v. 94, p. 10,937–10,954.
Mellor, G. L., and Yamada, T., 1974, A hierarchy of turbulence closure models for planetary boundary layers: Journal of Atmospheric Sciences, v. 31, p. 1791–1806.
———— 1982, Development of a turbulence closure model for geophysical fluid problems: Review of Geophysics and Space Physics, v. 20, p. 851–875.
Milliman, J. D., and Meade, R. H., 1983, World-wide delivery of river sediment to the oceans: Journal of Geology, v. 91, p. 1–21.
Morcos, S. A., 1970, Physical and chemical oceanography of the Red Sea: Annual Reviews of Oceanography and Marine Biology, v. 8, p. 73–202.
Munk, W. H., 1950, On wind-driven circulation: Journal of Meteorology, v. 7, p. 79–83.
Murray, J. W., 1991, Hydrographic variability in the Black Sea, *in* Izdar, E., and Murray, J. W., editors, Black Sea oceanography: NATO Advanced Science Institutes Series C, Mathematical and Physical Sciences Volume 351, p. 1–15.
Oey, L.-Y., G. L. Mellor, and R. I. Hires, 1985, A three-dimensional simulation of the Hudson-Raritan estuary. Part I: Description of the model and model simulations. Part II: Comparison with observation. Part III: Salt flux analyses: Journal of Physical Oceanography, v. 15, p. 1676–1720.
Parrish, J. T., and Guatier, D. L., 1993, Sharon Springs Member of Pierre Shale: upwelling in the Western Interior Seaway?, *in* Caldwell, W. G. E. and Kaufmann, E. G., editors, Evolution of the Western Interior Seaway: Geological Association of Canada Special Paper 39, p. 319–332.
Peixoto, J. P., and Oort, A. H., 1992, Physics of climate: New York, American Institute of Physics, 520 p.
Pickard, G. L., and Emery, W. J., 1983, Descriptive physical oceanography: New York, Pergamon Press, 249 p.
Pratt, L. M., 1984, Influence of paleoenvironmental factors on preservation of organic matter in Middle Cretaceous Greenhorn Formation, Pueblo, Colorado: American Association of Petroleum Geologists Bulletin, v. 68, p. 1146–1159.
———— 1985, Isotopic studies of organic matter and carbonate in rocks of the Greenhorn marine cycle, *in* Pratt, L. M., Kauffman, E. G., and Zelt, F. B., editors, Fine-grained deposits and biofacies of the Cretaceous Western Interior Seaway: Evidence for cyclic processes: Society of Economic Paleontologists and Mineralogists, Field Trip Guidebook 4, p. 38–48.
Reid, R. O., 1948, A model of the vertical structure of mass in equatorial wind-driven currents of a baroclinic ocean: Journal of Marine Research, v. 7, p. 62–91.
Richards, F. A., and Vaccaro, R., 1956, The Cariaco Trench, an anareobic basin in the Caribbean Sea: Deep Sea Research, v. 3, p. 214–228.
Roach, P. J., 1982, Computational fluid dynamics: Albuquerque, Hermosa, 446 p.
Ross, D. A., Uchipi, E., Prada, K. E., and MacIlvanin, J. C., 1974, Bathymetry and microtopography of Black Sea, *in* Ross, D. A., Degens and E. T., editors, The Black Sea, Geology, chemistry, and biology: American Association of Petroleum Geologists Memoir 20, p. 1–10.
Ryther, J. H., Menzel, D. W., and Corwin, N., 1967, Influence of the Amazon River outflow on the ecology of the western tropical Atlantic, I: hydrology and nutrient chemistry: Journal of Marine Research, v. 25, p. 69–82.
Schlanger, S. O., and Jenkyns, H. C., 1976, Cretaceous oceanic anoxic events—causes and consequences: Geologic en Mijnbouw, v. 55, p. 179–184.
Sheng, Y. P., and Lick, W., 1979, The transport and resuspension of sediments in a shallow lake: Journal of Geophysical Research, v. 84, p. 1809–1826.
Slater, R. D., 1985, A numerical model of tides in the Cretaceous Seaway of North America: Journal of Geology, v. 93, p. 333–345.

Smagorinsky, J., 1963, General circulation experiments with the primitive equations, I. The basic experiment: Monthly Weather Review, v. 91, p. 99–164.
Stommel, H., 1948, The westward intensification of wind-driven ocean currents: Transactions of the American Geophysical Union, v. 29, p. 202–206.
Takahashi, T., Broecker, W. S., and Langer, S., 1985, Redfield ratio based on chemical data form isopycnal surfaces: Journal of Geophysical Research, v. 90, p. 6907–6924.
Walsh, J. J., Dieterle, D. A., and Meyers, M. B., 1988, A simulation analysis of the fate of phytoplankton within the mid-Atlantic bight: Continental Shelf Research, v. 8, p. 757–787.
Weatherly, G., and Martin, P. J., 1978, On the structure and dynamics of the ocean bottom boundary layer, Journal of Physical Oceanography, v. 8, p. 557–570.
Weikert, H., 1987, Plankton and the pelagic environment, *in* Edwards, A. J., and Head, S. M., Red Sea: New York, Pergamon Press, p. 90–111.
Williams, G. D., and Stelck, C. R., 1975, Speculations on the Cretaceous paleogeography of North America, *in* Caldwell, W. G. E., editor, The Cretaceous System in the Western Interior of North America: Geological Association of Canada Special Paper 13, p. 1–20.
Winker, C. D., and Buffler, R. T., 1988, Paleogeographic evolution of early deep-water Gulf of Mexico and margins, Jurassic to Middle Cretaceous (Comanchean): American Association of Petroleum Geologists Bulletin, v. 72, p. 318–346.
Winterhalter, B., Floden, T., Ignatius H., Axberg, S., and Niemisto, L., 1981, Geology of the Baltic Sea, *in* Voipo, A., editor, The Baltic Sea: Elsevier Oceanography Series 30, p. 1–121.